Fast Synthesis of PbS Nanoparticles for Fabrication of Glucose Sensor with Enhanced Sensitivity

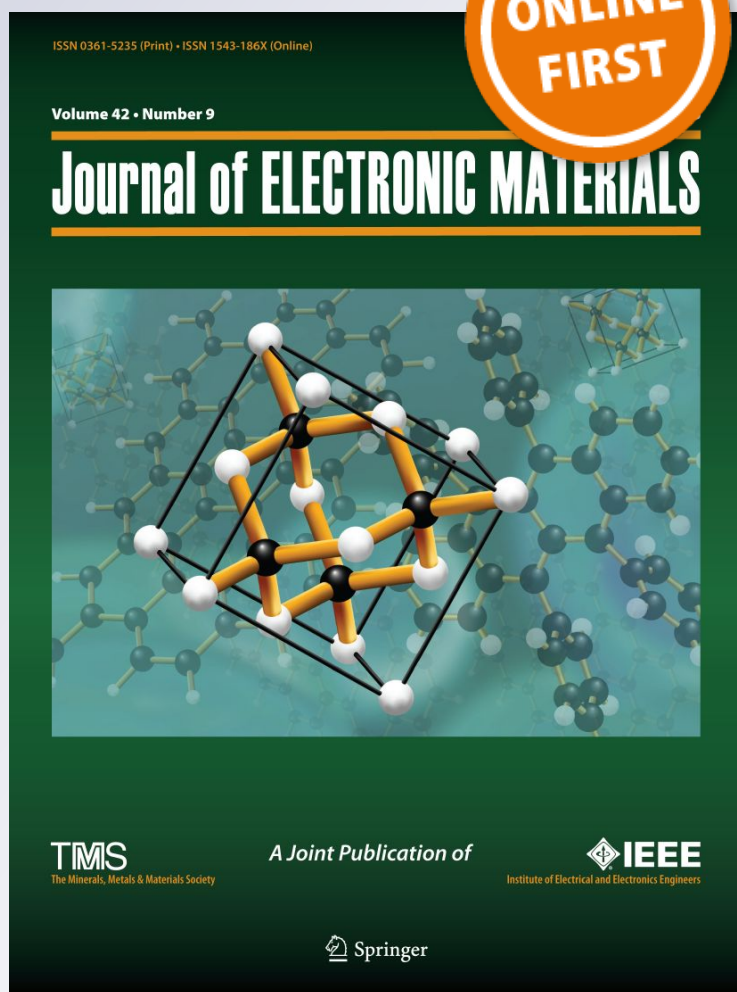Cong Doanh Sai, Manh Quynh Luu, Van Vu Le, Phuong Mai Nguyen, Nguyen Hai Pham, Viet Tuyen Nguyen, Xuan Quy Nguyen, Quoc Khoa Doan, et al.

ISSN 0361-5235 (Print) • ISSN 1543-186X (Online)

Volume 42 • Number 9

Journal of ELECTRONIC MATERIALS

ONLINE FIRST

TMS
The Minerals, Metals & Materials Society

A Joint Publication of

IEEE
Institute of Electrical and Electronics Engineers

Springer

Springer

CrossMark

Fast Synthesis of PbS Nanoparticles for Fabrication of Glucose Sensor with Enhanced Sensitivity

CONG DOANH SAI,[1] MANH QUYNH LUU,[1] VAN VU LE,[1]
PHUONG MAI NGUYEN,[1] NGUYEN HAI PHAM,[1]
VIET TUYEN NGUYEN,[1,5] XUAN QUY NGUYEN,[2]
QUOC KHOA DOAN,[3,6] and THI HA TRAN[4]

1.—Faculty of Physics, Vietnam National University – University of Science, 334 Nguyen Trai, Thanh Xuan, Hanoi, Vietnam. 2.—Bac Ha International University, Lim Town, Tien Du District, Bac Ninh Province, Vietnam. 3.—Duy Tan University, 182 Nguyen Van Linh, Danang, Vietnam. 4.—Faculty of General Sciences, Hanoi University of Mining and Geology, Tu Liem, Hanoi, Vietnam. 5.—e-mail: nguyenviettuyen@hus.edu.vn. 6.—e-mail: doanquockhoa2016@gmail.com

PbS nanoparticles with average size of 12 nm have been synthesized by a novel time-saving method that combines sonochemical and laser postannealing processes, the latter being important for improved crystal quality of the nanoproduct. The crystalline quality and morphology of the PbS nanoparticles were characterized using several techniques such as Raman spectroscopy, x-ray diffraction analysis, transmission electron microscopy, diffuse reflectance spectroscopy, and energy-dispersive x-ray analysis. The as-produced PbS nanoproduct was then used to make a glucose sensor. Electrochemical measurements showed that the sensitivity of the glucose sensor based on PbS nanoparticles was 546.2 μA cm^{-2} mM^{-1}, much higher than for glucose sensors based on other semiconductor materials reported in literature.

Key words: Lead sulfide, nanoparticles, laser annealing, sonochemical, glucose sensor

INTRODUCTION

As an important group IV–VI semiconductor, lead sulfide (PbS) has attracted considerable attention due to its unique properties such as narrow direct bandgap (0.41 eV at 300 K) and large Bohr exciton radius (20 nm).[1,2] PbS has long been used in a wide range of electronic applications including sensors, phototransistors, solar absorbers, etc.[3–5] Over the past few decades, interest in PbS from materials scientists and engineers has shifted to fabrication of nanostructures, thanks to their enhanced surface and quantum properties, which cannot be attained in bulk counterpart materials. Various methods have been used to fabricate PbS nanostructures, for example, chemical deposition, electrodeposition, photochemical methods, vacuum deposition, etc.[6–13] Among these, solution growth using the general or sonochemical method in particular shows various advantages, including low cost, high efficiency, and easy production scaling. However, such methods have not always produced high-quality products. We present herein a fast and convenient process combining sonochemical synthesis and laser treatment to produce high-quality PbS nanoparticles efficiently. The average size of the as-prepared PbS was approximately 12 nm. The products were characterized by x-ray powder diffraction (XRD) analysis, Raman spectroscopy, transmission electron microscopy (TEM), high-resolution transmission electron microscopy (HRTEM), selected-area electron diffraction (SAED), and diffuse reflectance spectroscopy. A glucose sensor was then fabricated based on the obtained PbS nanoparticles. The sensor was characterized by electrochemical measurements, which showed high sensitivity. These results suggest that PbS nanoparticles are promising for fabrication of low-cost, high-sensitivity glucose sensors.
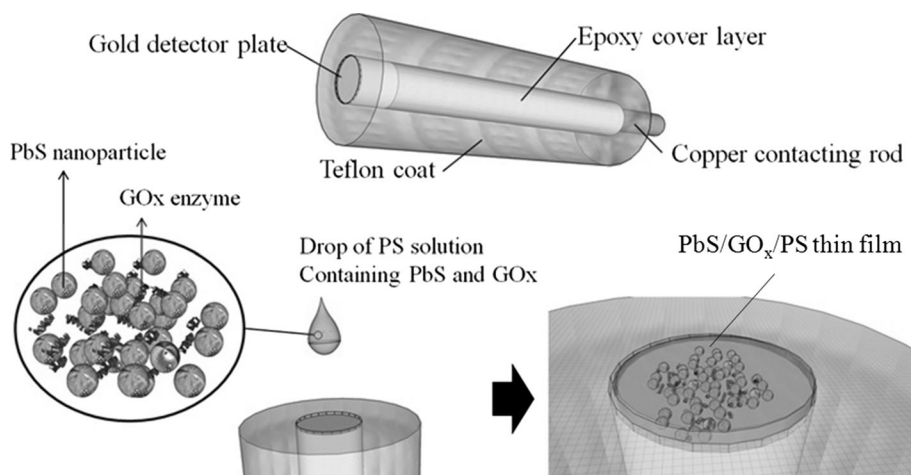
Fig. 1. Schematic diagram of PbS/GOx/PS working electrode.

EXPERIMENTAL PROCEDURES

PbS Nanoparticle Preparation and Characterization

Lead sulfide nanoparticles were synthesized by a sonochemical method followed by laser postannealing. The starting chemical regents were $Pb(CH_3COO)_2$ (99%), thioacetic acid (TAA, 99%), and cetyltrimethylammonium bromide (CTAB, 99.8%). Chemical regents were obtained from Merck (Germany) and used without any further purification. In a typical process, 20 ml 0.25 M $Pb(CH_3COO)_2$, 20 ml 0.6 M TAA, and 10 ml 0.06 M CTAB were mixed together. The solution was ultrasonicated using a titanium horn (VCX 750 ultrasonic generator, 20 kHz). The reaction took place under nitrogen ambient atmosphere to minimize oxidation that could affect the product. After 10 min, a black precipitate formed and was collected by centrifugation. After being washed and dried, the product was postannealed using a 632.8-nm laser beam, in vacuum to prevent oxidation of the product. The annealing process was performed in several cycles, each of which lasted for 30 s.

The evolution of the crystal structure of the PbS nanoproduct during annealing was observed by Raman spectroscopy (Horiba LabRAM HR800) at excitation wavelength of 632.8 nm. The crystal structure of the PbS nanoproduct was analyzed by x-ray diffractometer (Siemens D5005, Bruker, Germany) with Cu $K_{\alpha 1}$ ($\lambda = 0.154056$ nm) radiation. The morphology of the nanoparticles was characterized by high-resolution transmission electron microscope (FEI Tecnai TF20 FEG). The composition of the sample was determined by energy-dispersive x-ray (EDX) spectrometry (Oxford Isis 300) integrated into a JEOL-JSM 5410 scanning electron microscope. Diffuse reflectance spectra of the PbS powder were collected using a Cary 5000 ultraviolet–visible–near infrared (UV–Vis-NIR) spectrophotometer.
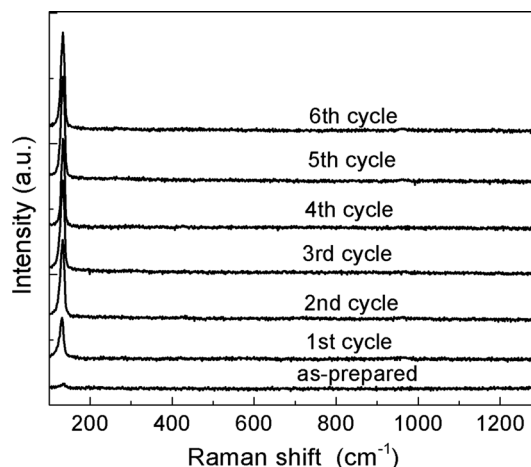

Fig. 2. Evolution of Raman spectrum of PbS nanoparticles during laser annealing.

Electrochemical Measurement Setup for Glucose Sensor

The working electrode (WE) for the electrochemical glucose sensing measurements was a 3-mm-diameter circular gold plate (Fig. 1). The electrode was cleaned using 0.1 M HCl and 0.1 M NaOH solutions in sequence. A drop of polystyrene (PS) in dichloromethane (CH_2Cl_2) containing 400 units glucose oxidase (GOx) and 1 mg PbS was then dropped onto the electrode. After the CH_2Cl_2 had completely evaporated, a PbS/GOx/PS thin film was formed to serve as an electron receptor.

The electrochemical cell was set up with the as-prepared working electrode, a platinum counterelectrode (CE), and a saturated Ag/AgCl reference electrode. The distance between the working electrode and counterelectrode was 15 mm. The glucose concentration was increased from 0.1 mM to 1.3 mM to simulate the range of blood sugar levels

Fast Synthesis of PbS Nanoparticles for Fabrication of Glucose Sensor with Enhanced Sensitivity

in the human body. A cyclic potential voltage was applied from 0 V to 1.5 V in steps of 0.01 V at scan rate of 50 mV/s.
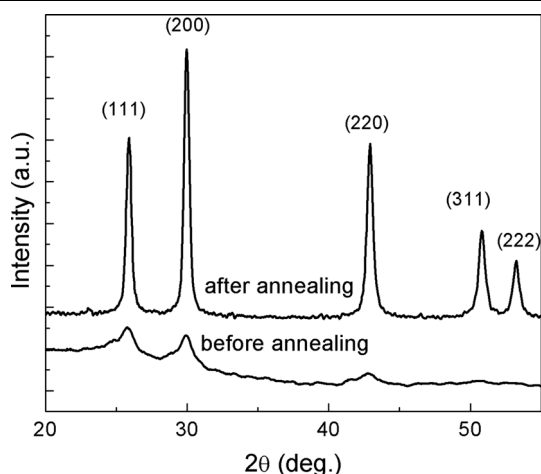

Fig. 3. XRD patterns of PbS nanoparticles before and after laser treatment.
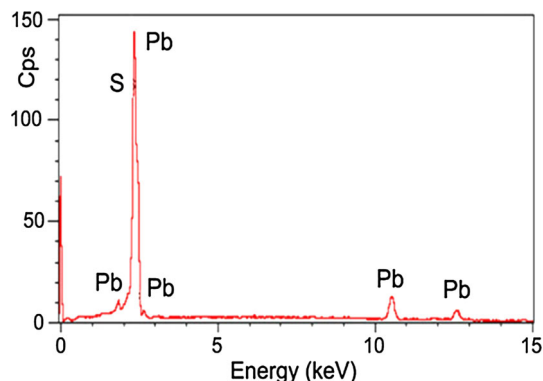

Fig. 4. EDX spectrum of PbS nanoparticles after laser annealing.

RESULTS AND DISCUSSION

Solution growth techniques from aqueous solution in general and using the sonochemical method in particular show various advantages including low cost, high efficiency, and ease of production scaling. However, such methods do not always offer high-quality products. In this work, it was found that the crystal quality was improved by laser annealing, which offers many advantages compared with conventional annealing methods.[14] In this section, the laser annealing treatment is discussed in detail.

PbS is sensitive to photodecomposition, meaning that PbS nanoparticles can be turned into other substances containing oxygen, such as PbO or lead sulfate, according to Yousefi et al.[15] and Blackburn et al.[16] To eliminate the possibility of photodegradation during laser annealing, the laser treatment was performed in a vacuum chamber in several cycles, each of which lasted for 30 s. After each cycle, the sample was examined *in situ* by Raman spectroscopy. The power density used in the Raman measurements was also kept low to avoid heating during the acquisition time. The evolution of the Raman spectrum of the PbS nanoparticles during laser annealing is shown in Fig. 2. Only one sharp peak at 133 cm^{-1} was observed, which can be assigned to either the vibration mode of PbO[17] or a combination of the transverse acoustic (TA) and transverse optical (TO) phonon modes of PbS.[18] As the annealing process and Raman measurements were performed in vacuum, the first explanation is not likely. The lack of the characteristic Raman peak at around 960 cm^{-1} corresponding to lead sulfate, which usually accompanies lead oxide,[16] supports the assignment of the observed Raman peak to vibration of the PbS lattice. In addition, the lack of formation of PbO or $PbSO_4$ was confirmed by XRD and EDX measurements on the annealed sample. As seen from the Raman spectra in Fig. 2,
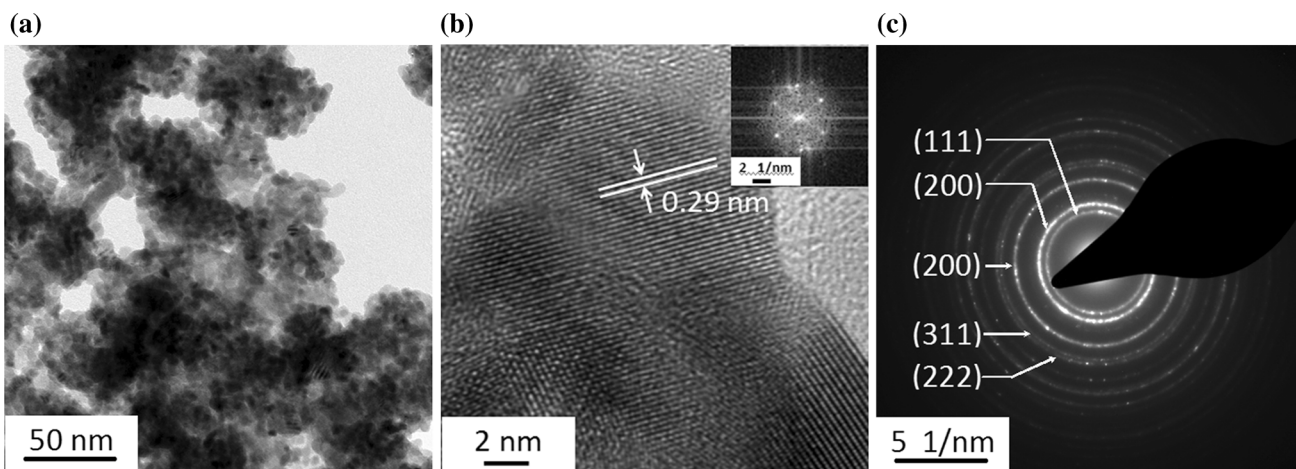

Fig. 5. (a) TEM and (b) HRTEM images and (c) SAED image of PbS nanocrystals. The inset in (b) shows the fast Fourier transform pattern of the HRTEM image.

the crystal quality of the sample was clearly improved after the first cycle and continued to improve after several subsequent cycles. The Raman intensity almost reached saturation after six cycles, suggesting that treatment could be finished after 3 min.

The effect of annealing was confirmed based on the XRD patterns of the sample before and after laser treatment, as presented in Fig. 3. The XRD pattern of the sample before postannealing consisted of several characteristic peaks of lead sulfide at 25.7°, 29.8°, 42.7°, and 50.6°, corresponding to (111), (200), and (220) lattice planes of the PbS face-centered cubic structure. Besides, the XRD pattern of the sample before annealing showed a broad baseline, which probably indicates presence of some amorphous material. The XRD results imply that PbS nanoparticles were formed after the sonochemical process, but some amorphous PbS material was also present in the product. The disappearance of the broad baseline in the XRD pattern after laser treatment indicates that the amorphous phase in the product was transformed into crystalline material. The sharper diffraction peaks of the final product also demonstrate the important role of laser annealing in improving the crystal quality of the PbS nanoparticles.

It is also important to note that no peaks related to PbO or $PbSO_4$ were observed for the annealed sample, again excluding formation of unwanted phases such as PbO and $PbSO_4$. The lattice constant of the final product, as determined from the XRD pattern, was $a = 5.93(3)$ Å, in good agreement with the value of 5.936 Å reported in Joint Committee on Powder Diffraction Standards (JCPDS) ICDD1993 card no. 5-592. Crystal size of about 11 nm was obtained from the Debye–Scherrer relation,[19]

$$L = \frac{0.9}{B \cos \theta},\qquad(1)$$

where B, θ, and λ are the full-width at half-maximum (FWHM) in radians of the diffraction peak, the Bragg diffraction angle, and the wavelength of the $K_{\alpha 1}$ component of the employed copper radiation (1.54056 Å), respectively. Furthermore, the EDX spectrum shown in Fig. 4 indicates that the PbS sample contained only Pb and S elements; other impurities, if any, were present below the detection limit of the EDX measurements.

A typical TEM and HRTEM image and SAED pattern of the PbS nanoparticles are shown in Fig. 5. TEM imaging showed that the nanoparticles had quasispherical shape with average size of about 12 nm and were well separated from each other. Figure 5b shows a magnified HRTEM image of PbS
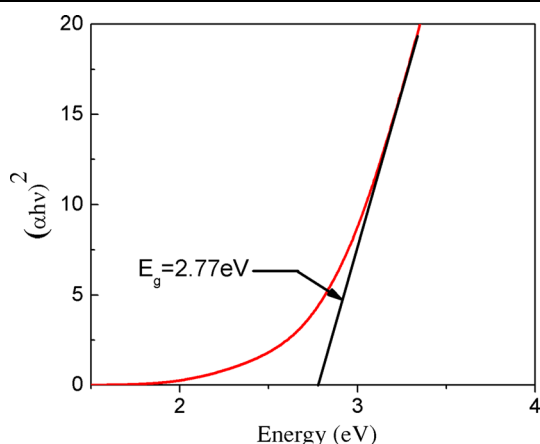

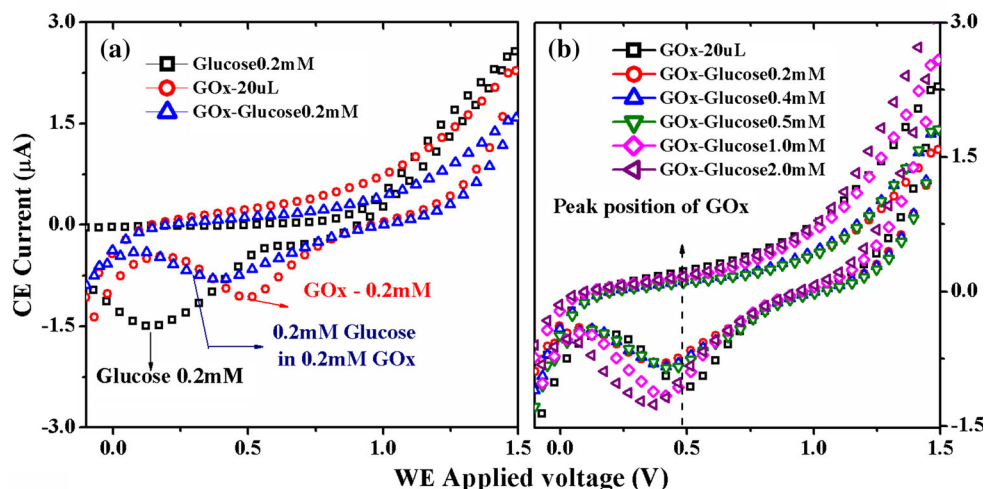Fig. 6. $(\alpha h\nu)^2$ versus $h\nu$ for PbS nanopowder.

Fig. 7. Role of glucose oxidase (GOx) investigated by cyclic voltammetry. (a) CV diagrams of 0.2 mM glucose, 0.2 mM GOx, and 0.2 mM glucose in 0.2 mM GOx-containing solution. (b) CV diagrams for different concentrations of glucose (0.2 mM, 0.4 mM, 1 mM, and 2 mM) in 0.2 mM GOx. All CV measurements were performed with gold working electrode.

Fast Synthesis of PbS Nanoparticles for Fabrication of Glucose Sensor with Enhanced Sensitivity
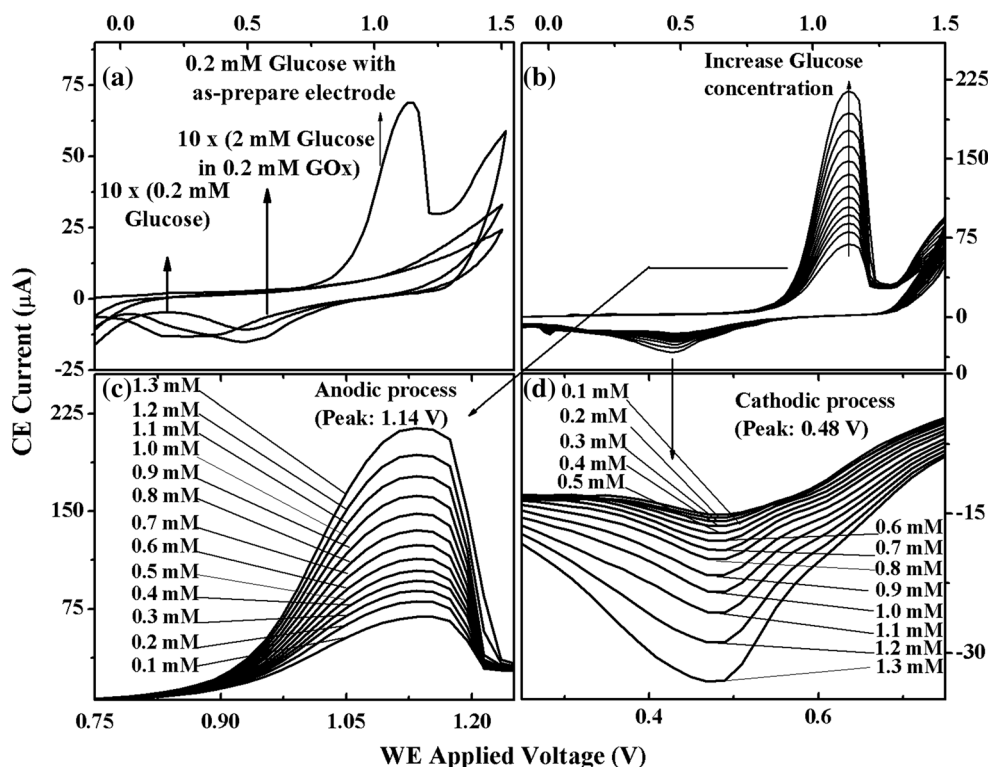

Fig. 8. CV investigation of PbS-nanoparticle-based WE at different glucose concentrations: (a) CV diagrams of 0.2 mM glucose, 2 mM glucose in 0.2 mM GOx with gold WE, and 0.2 mM glucose with PbS-based WE. (b) CV diagrams of glucose solution at different concentrations (0.1 mM to 1.3 mM) with PbS-based WE. (c, d) Selected regions from anodic process and cathodic process taken from the CV diagrams in (b).
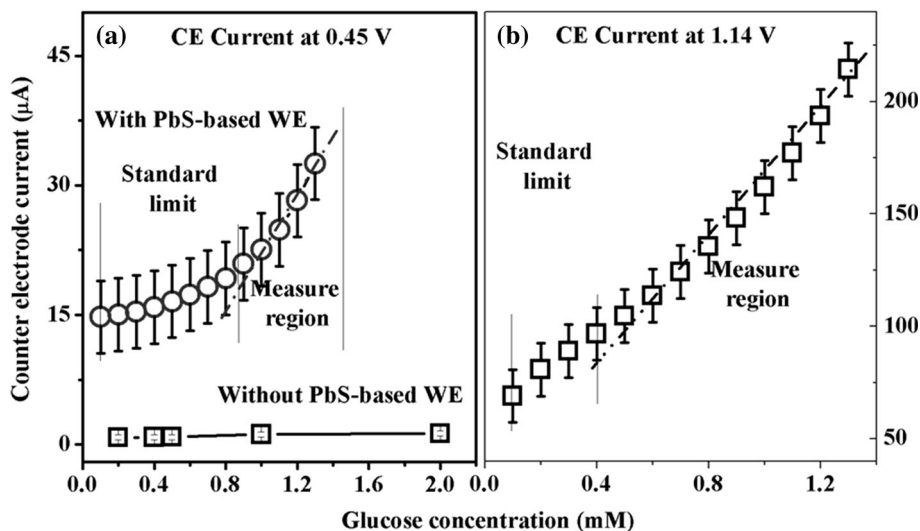

Fig. 9. Glucose concentration dependence of CE current at 0.45 V, evaluated from CV diagrams obtained with and without PbS-based electrode (a) and at 1.14 V from the CV diagram obtained with PbS-based electrode (b).

nanoparticles, revealing lattice fringes of (200) planes with spacing of 2.9 Å, coinciding with the value obtained by XRD analysis. The fast Fourier transform pattern of the HRTEM image (Fig. 5b, inset) also confirms the face-centered cubic structure of the PbS nanoparticles. The SAED image in Fig. 5c consists of diffraction rings, indicating that the PbS nanocrystals were arranged with random orientation.

The absorption of the PbS sample was obtained from diffuse reflectance values using the Kubelka–Munk function,[20]

$$F(R) = \frac{(1-R)^2}{2R} = \frac{K}{S}, \tag{2}$$

where R, K, and S are the reflection, absorption, and scattering coefficient, respectively. The bandgap of the PbS nanoproduct was then estimated using the following equation for a direct transition:

$$\alpha h v = A(h - E_g)^{1/2}, \tag{3}$$

where A is a constant and E_g is the bandgap of the material. A plot of $(\alpha h v)^2$ versus $h v$ for the PbS nanocrystals is presented in Fig. 6. Extrapolating the straight portion of the graph to the energy axis at $\alpha = 0$ gives a bandgap for PbS of 2.77 eV. This value, which is much larger than that of bulk PbS, indicates that the PbS nanocrystals exhibit the quantum confinement effect due to the reduction of the crystal size to below the Bohr exciton radius.

In $1\times$ phosphate-buffered saline (PBS) medium, a glucose–GOx complex is formed following specific conjugation of glucose oxidase enzyme and a glucose molecule. Figure 7 presents cyclic voltammetry (CV) results to detect the presence of this complex in PBS. As shown in Fig. 7a, one peak was observed at 0.14 V on the oxidation curve of the CV diagram for pure glucose in PBS, which might correspond to glucose oxidation. When the solution contained only glucose oxidase enzyme, another peak was observed at 0.49 V. Other observations of GOx oxidation, in 0.05 M PBS with a Nafion-modified electrode,[21] showed a peak at 0.4 V. The different position of this peak may result from the fact that $1\times$ PBS was used in this study instead of Nafion. When 0.2 mM of glucose–GOx mixture was added to the PBS solution, a slight shift of the peak position from 0.49 V to 0.45 V was observed. Such a change was also reported by Madhu et al.,[22] who attributed the peak shift to interaction between glucose and GOx molecules.[21,22] When increasing the glucose concentration, the cross-section for the GOx–glucose interaction increases, resulting in an increase of the oxidation peak current for the glucose–GOx complex, followed by a shift of the peak position to lower values (Fig. 7b).

The CV diagram for 0.2 mM glucose observed with the PbS-modified electrode is shown in Fig. 8a. Compared with the CV diagram for the glucose–GOx complex obtained with bare gold electrode (red line), it is observed that the oxidation peak of glucose–GOx increased by 12 times, while a reduction peak occurred on the reduction curve at 1.14 V. Cyclic voltammetry of galena was also investigated, showing a broad peak at 0.9 V, which corresponds to the transformation of PbS to $HPbO_2^-$.[23] A shift of the reduction energy was detected in this study, which might be related to the polystyrene cover and/or the presence of PbS. Regarding the current amplification at the 0.45 V peak of the glucose–GOx oxidation, good agreement was found with other articles,[21,22] indicating that the nanostructure

created an electron-transmitting framework which directly transferred the reduced electron from the glucose–GOx complex to the electrode.

As the glucose concentration was increased, the anodic current at 1.14 V (Fig. 8c) and the cathodic current at 0.45 V (Fig. 8d) increased. This can be understood based on the fact that, as the number of glucose molecules was increased, the probability of bond formation between glucose and GOx molecules augmented, improving the number of electrons transferred to the electrode.

The cathodic current at 0.45 V obtained from the oxidation curves measured at different glucose concentrations with and without the PbS-modified electrode is presented in Fig. 9a as a function of glucose concentration. The dependence of the anodic current at 1.14 V from the reduction curve on the glucose concentration is shown in Fig. 9b. It should be noted that, with the PbS-nanoparticle-modified electrode, the rise in the cathodic current at 0.45 V was much greater than when PbS was not used. Besides, the peak current at 1.14 V showed higher sensitivity to glucose than the peak at 0.45 V. The sensor sensitivity, calculated from the intensity increase of the 1.14 V peak, was 546.2 $\mu A\ cm^{-2}\ mM^{-1}$, being high compared with previously reported data.[24–30]

GOx molecules are usually found to be 580 to 585 residues long, with three sulfur atom (S)-containing hydrophilic cysteines at positions 164, 206, and 512. Position 512 is near the edge of the N-domain and close to the flavin adenine dinucleotide linking position. A possible mechanism for the increase in the sensitivity of the biosensor would be direct transfer of an electron from the mediator material to the molecules. Meanwhile, metal sulfide nanocrystals could easily link to the S atom of the organic molecules via a stable covalent bond.[31] Such direct linkage of the material to the S atom in residue 512 may induce electron transfer from GOx to the electrode and consequently explain the sensitivity enhancement reported herein.

CONCLUSIONS

Using a sonochemical method combined with laser postannealing, we successfully prepared high-quality PbS nanoparticles. Laser annealing helped to save time and energy compared with conventional annealing methods and played a critical role in greatly improving the crystal quality of the as-prepared nanoproduct. The nanoproduct was then used as an electron receptor in a glucose sensor, which exhibited much higher sensitivity compared with the same type of sensor based on other semiconductors. Direct linkage of the nanoparticles to glucose oxidase is believed to be responsible for the high sensitivity of the glucose sensor reported herein, although the exact mechanism for the sensitivity enhancement of the glucose sensor based on PbS nanoparticles should be subject to further study.

Fast Synthesis of PbS Nanoparticles for Fabrication of Glucose Sensor with Enhanced Sensitivity

REFERENCES

1. O. Madelung, U. Rössler, and M. Schulz, *Non-Tetrahedrally Bonded Elements and Binary Compounds I*, 1st ed. (Berlin: Springer, 1998), pp. 874–889.
2. A.H. Khan, U. Thupakula, A. Dalui, S. Maji, A. Debangshi, and S. Acharya, *J. Phys. Chem. C* 117, 7934 (2013).
3. Y. Luo, C. Dong, X. Li, and Y. Tian, *J. Electroanal. Chem.* 759, 51 (2015).
4. M. Asad, M. Fathipour, M.H. Sheikhi, and M. Pourfath, *Sens. Actuators A* 220, 213 (2014).
5. W. Yoon, J.E. Boercker, M.P. Lumb, D. Placencia, E.E. Foos, and J.G. Tischler, *Sci. Rep.* (2013). doi: 10.1038/srep02225.
6. J.H. Warner, E. Thomsen, A.R. Watt, N.R. Heckenberg, and H. Rubinsztein-Dunlop, *Nanotechnology* 16, 175 (2005).
7. L. Xu, W.Q. Zhang, Y.W. Ding, W.C. Yu, J.Y. Xing, F.Q. Li, and Y.T. Qian, *J. Cryst. Growth* 273, 213 (2004).
8. S.M. Lee, Y.W. Jun, S.N. Cho, and J.W. Cheon, *J. Am. Chem. Soc.* 124, 11244 (2002).
9. Y. Zhao, X.H. Liao, J.M. Hong, and J.J. Zhu, *Mater. Chem. Phys.* 87, 149 (2004).
10. N.B. Egorov, L.P. Eremin, V.F. Usov, and A.M. Larionov, *High Energy Chem.* 41, 251 (2007).
11. A. Carrillo-Castillo, R.C. Ambrosio Lázaro, A. Jimenez-Pérez, C.A. Martínez Pérez, E.C. de la Cruz Terrazas, and M.A. Quevedo-López, *Mater. Lett.* 121, 19 (2014).
12. Ü.Ç. Üst, K. Dağcı, and M. Alanyalıoğlu, *Mater. Sci. Semicond. Process.* 41, 270 (2016).
13. N.I. Fainer, M.L. Kosinova, Yu.M. Rumyantsev, E.G. Salman, and F.A. Kuznetsovh, *Thin Solid Films* 280, 16 (1996).
14. T.H. Tran and V.T. Nguyen, *Mater. Sci. Semicond. Process.* 46, 6 (2016).
15. R. Yousefi, M. Cheraghizade, F. Jamali-Sheini, W.J. Basirun, and N.M. Huang, *Curr. Appl. Phys.* 14, 1031 (2014).
16. J.L. Blackburn, H. Chappell, J.M. Luther, A.J. Nozik, and J.C. Johnson, *J. Phys. Chem. Lett.* 2, 599 (2011).
17. R. Sherwin, R.J.H. Clark, R. Lauck, and M. Cardona, *Solid State Commun.* 134, 565 (2005).
18. C. Huaqiang, W. Guozhi, Z. Sichun, and Z. Xinrong, *Nanotechnology* 17, 3280 (2006).
19. B.E. Warren, *X-ray Diffraction*, 1st ed. (New York: Dover, 1990), pp. 253–254.
20. N.N. Yamashita, *J. Phys. Soc. Jpn.* 35, 1089 (1973).
21. Q. Liu, X. Lu, J. Li, X. Yao, and J. Li, *Biosens. Bioelectron.* 22, 3203 (2007).
22. R. Madhu, B. Devadas, S.M. Chen, and M. Rajkumar, *ACS Anal. Methods* 6, 9053 (2014).
23. A.S. Cuharuc, L.L. Kulyuk, R.I. Lascova, A.A. Mitioglu, and A.I. Dikusar, *Surf. Eng. Appl. Electrochem.* 48, 193 (2012).
24. A. Wei, X.W. Sun, J.X. Wang, Y. Lei, X.P. Cai, C.M. Li, Z.L. Dong, and W. Huang, *Appl. Phys. Lett.* (2006). doi: 10.1063/1.2356307.
25. J. Zang, C.M. Li, X. Cui, J. Wang, X. Sun, H. Dong, and C.Q. Sun, *Electroanalysis* 19, 1008 (2007).
26. H. Yang and Y. Zhu, *Biosens. Bioelectron.* 22, 2989 (2007).
27. D.H. Yang, N. Takahara, S.W. Lee, and T. Kunitake, *Sens. Actuators B Chem.* 130, 379 (2008).
28. C. Li, Y. Liu, L. Li, Z. Du, S. Xu, M. Zhang, X. Yin, and T. Wang, *Talanta* 77, 455 (2008).
29. A. Umar, M.M. Rahman, and Y.B. Hahn, *Electrochem. Commun.* 11, 1353 (2009).
30. L.C. Jiang and W.D. Zhang, *Biosens. Bioelectron.* 25, 1402 (2010).
31. N.T. Trang, L.M. Quynh, T.V. Nam, and H.N. Nhat, *Surf. Sci.* 608, 67 (2013).